JACS
JOURNAL OF THE AMERICAN CHEMICAL SOCIETY
Article
pubs.acs.org/JACS

Effective Optical Faraday Rotations of Semiconductor EuS Nanocrystals with Paramagnetic Transition-Metal Ions

Yasuchika Hasegawa,*[,†] Masashi Maeda,[†] Takayuki Nakanishi,[†] Yoshihiro Doi,[‡] Yukio Hinatsu,[‡] Koji Fujita,[§] Katsuhisa Tanaka,[§] Hitoshi Koizumi,[†] and Koji Fushimi[†]

[†]Faculty of Engineering and [‡]Faculty of Science, Hokkaido University, N13 W8, Kita-ku, Sapporo, Hokkaido 060-8628, Japan
[§]Graduate School of Engineering, Kyoto University, Katsura, Nishikyo-ku, Kyoto 615-8510, Japan

Supporting Information

ABSTRACT: Novel EuS nanocrystals containing paramagnetic Mn(II), Co(II), or Fe(II) ions have been reported as advanced semiconductor materials with effective optical rotation under a magnetic field, Faraday rotation. EuS nanocrystals with transition-metal ions, EuS:M nanocrystals, were prepared by the reduction of the Eu(III) dithiocarbamate complex tetraphenylphosphonium tetrakis-(diethyldithiocarbamate)europium(III) with transition-metal complexes at 300 °C. The EuS:M nanocrystals thus prepared were characterized using X-ray diffraction (XRD), transmission electron microscopy (TEM), inductively coupled plasma atomic emission spectroanalysis (ICP-AES), and a superconducting quantum interference device (SQUID) magnetometer. Enhanced Faraday rotations of the EuS:M nanocrystals were observed around 550 nm, and their enhanced spin polarization was estimated using electron paramagnetic resonance (EPR) measurements. In this report, the magneto-optical relationship between the Faraday rotation efficiency and spin polarization is discussed.

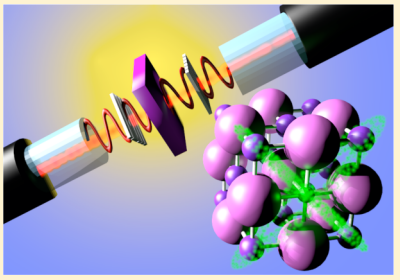

INTRODUCTION

The optical Faraday effect causes rotation of the plane of polarized light, which is linearly proportional to the component of the magnetic field in the direction of propagation. This characteristic Faraday effect is important for the construction of optical isolators for fiber-optic telecommunication systems.[1] Various types of magneto-optical materials showing the Faraday effect have been reported over the past few decades.[2−13] In particular, the preparation of semiconductor nanocrystals with magnetic dopants has been investigated for the development of optical isolator and magneto-optical devices, and stochastic control for a number of magnetic dopants in II−VI or III−V semiconductor nanocrystals has been investigated. A semiconductor nanocrystal with magnetic dopants is a promising material for future magneto-optical devices such as an optical isolator.

One of the most important series of intrinsic semiconductors with magnetic properties is the europium chalcogenide family, EuX (X = O, S, Se, Te).[14] The characteristic Faraday effect of the semiconductor EuX comes from localized 4f electrons distributed between the conduction band (5d orbitals of Eu(II)) and the valence band (p orbitals of chalcogenides, O^{2-}, S^{2-}, Se^{2-}, or Te^{2-}).[15] The 4f−5d electronic transition and spin configuration of EuX crystals lead to a large Faraday effect, which makes these materials promising candidates for an effective optical isolator.[16−23] The characteristic Faraday effect in EuX crystals is markedly enhanced in nanoscale structures due to quantum confinement effects on the electronic excited states.[16−23] Nanoscale EuX crystals, or EuX nanocrystals, have been synthesized, and their resulting magneto-optical properties have been explored.[16−35] In particular, EuS nanocrystals are distinctly characterized by their ferromagnetic properties and characteristic Faraday effect in the visible region. EuS nanocrystals are expected to be useful in applications such as advanced optical isolators and spintronic devices using green and red laser light.

The magnitude of the Faraday rotation angle is directly linked to the magnetic behavior and related to spin polarization in the ground and excited states of magnetic materials. Effective Faraday rotation in EuS nanocrystals requires that the characteristic spin structure and spin configuration of EuS nanocrystals be improved by the addition of extra metal ions. Moruzzi and Gambino showed that the magnetic specific heat of Gd ion doped EuS bulk crystal is shifted to a higher temperature.[36,37] Stoll and Jin also studied enhancement of the Curie temperature of nanosized Gd ion doped EuS.[32,33] On the basis of these previous reports, the Gd ion can be regarded as an effective dopant for enhancement of the magnetic properties of EuS crystals. Remarkable magnetic polarona based on the 4f−5d exchange interaction of EuO bulk crystals with Gd ions have been also reported.[38] The Gd ion is one of the key materials for enhancement of magnetic properties in EuX crystals.

Generally, the trivalent gadolinium cation, Gd(III) ion, is used as the source for doping Gd ions in EuS crystals. The standard reduction potential of the Gd(III)/Gd(II) equilibrium in water has been reported to be $E° = -2.40$ V (SCE).[39] The

Received: October 29, 2012
Published: January 23, 2013

 © 2013 American Chemical Society dx.doi.org/10.1021/ja3106253 | J. Am. Chem. Soc. 2013, 135, 2659−2666

reduction potential is located in the less noble position in comparison to the reduction potential of Eu(III)/Eu(II) (E° = −0.43 V; SCE).[39] The less noble reduction potential of Gd(III)/Gd(II) indicates that the divalent Gd(II) ion is unstable at room temperature in air. The chemical reaction of the stable trivalent Gd(III) ion with S^{2-} leads to the formation of various gadolinium sulfides, such as orthorhombic Gd_2S_3, hexagonal Gd_3S_4, and tetragonal $GdS_{1.8}$ composed of Gd(III) ions. Park and co-workers also recently reported GdS nanocrystals composed of trivalent Gd(III) ions.[40] Gd(III) is a type of lanthanide ion, with a coordination number known to vary from 6 to 12 depending on the nature of the ligating element, such as oxygen, sulfur, and nitrogen.[41−43] On the basis of electrochemical analysis, synthesis experiments, and coordination structures, trivalent Gd(III) ions with a polyhedral coordination structure may be contained in EuS cubic nanocrystals. The trivalent Gd(III) ions in the vacancy of the divalent Eu(II) ion provide unstable charge and structural strains in the EuS cubic lattice. These strains in semiconductor nanocrystals directly promote the decrease of the magnetic moment and coercive field. Instead of the trivalent Gd(III) ion, a stable divalent metal ion with a six-coordinated structure and paramagnetic properties is expected to be a promising dopant for the enhancement of magnetic properties and for obtaining the Faraday effect in EuS nanocrystals.

Here, we focus on a stable divalent transition-metal ion with paramagnetic properties as an ideal dopant for effective Faraday rotation in EuS nanocrystals. Among the transition-metal ions, paramagnetic Mn(II), Co(II), and Fe(II) ions are well-known as magnetic dopant ions in semiconductors.[44] These transition-metal ions show stable six-coordinated structures in the solid crystal lattice. The paramagnetic Mn(II), Co(II), and Fe(II) ions could be the most suitable as dopants for improving the Faraday effect in EuS nanocrystals. In this study, we report novel EuS nanocrystals with paramagnetic transition-metal ions with divalent cations, EuS:M nanocrystals. The EuS:M nanocrystals were prepared by the reduction of the Eu(III) dithiocarbamate complex tetraphenylphosphonium tetrakis(diethyldithiocarbamate)europium(III) ($(PPh_4)[Eu(S_2CNEt_2)_4]$) with Mn(II), Co(II), and Fe(II) dithiocarbamate complexes ($[Mn(S_2CNEt_2)_2]$, $[Co(S_2CNEt_2)_2]$, and $[Fe(S_2CNEt_2)_2]$), as shown in Figure 1. The prepared EuS nanocrystals with paramagnetic Mn(II), Co(II), and Fe(II) ions, EuS:M, were characterized by X-ray diffraction (XRD), transmission electron microscopy (TEM), inductively coupled plasma atomic emission spectroanalysis (ICP-AES), and a superconducting quantum interference device (SQUID) magnetometer. Enhanced Faraday rotations in the EuS:M nanocrystals were observed around 550 nm. We also successfully estimated enhanced spin polarization using electron paramagnetic resonance (EPR) measurements.

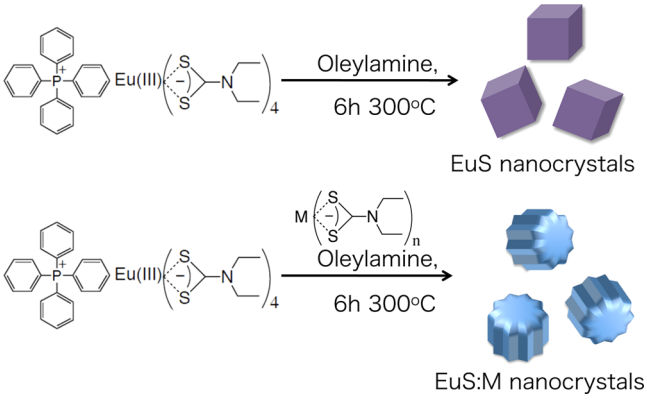

Figure 1. Preparation schemes of EuS and EuS:M nanocrystals.

In this study, we suggest that a large Faraday rotation efficiency is based on spin polarization related to the characteristic coercive field, although the magnetic moment and Curie point of the magnetic semiconductor have been previous areas of focus. Novel EuS:M nanocrystals with enhanced Faraday rotation efficiency are demonstrated for the first time.

EXPERIMENTAL SECTION

Materials. Europium(III) chloride hexahydrate ($EuCl_3·6H_2O$), manganese chloride tetrahydrate ($MnCl_2·4H_2O$), iron chloride tetrahydrate ($FeCl_2·4H_2O$), and cobalt chloride tetrahydrate ($CoCl_2·4H_2O$) were purchased from Kanto Chemical Co., Inc. Sodium *N*,*N*-diethyldithiocarbamate trihydrate ($Na(S_2CNEt_2)·3H_2O$) and toluene were purchased from Kanto Chemical Co., Inc. Tetraphenylphosphonium bromide ($BrPPh_4$) was purchased from Wako Pure Chemical Industries, Ltd. Oleylamine was obtained from Tokyo Chemical Industry Co., Ltd. All other chemicals and solvents were reagent grade and were used without further purification.

Apparatus. ^{1}H NMR data were measured using a JEOL JNM-EX270 (270 MHz) instrument. ^{1}H NMR chemical shifts were determined using tetramethylsilane (TMS) as an internal standard. Infrared spectra were recorded on a JASCO FT/IR-350 spectrometer. Elemental analyses were performed with a Yanaco MT-6 CHN corder. XRD spectra were characterized by a Rigaku RINT 2200 X-ray diffractometer. High-resolution images of the EuS nanocrystals were obtained with a JEOL 2010 FASTEM (200 kV) TEM. Quantitative elemental analysis was performed with ICP-AES. Magnetic measurements were carried out using a Quantum Design MPMS SQUID system. Electron paramagnetic resonance spectra of EuS:M nanocrystals were measured using a JEOL JES-TE200 ESR spectrometer.

Synthesis of Tetraphenylphosphonium Tetrakis(diethyldithiocarbamate)europium(III), $(PPh_4)[Eu(S_2CNEt_2)_4]$. A solution of sodium dithicarbamate trihydrate ($Na(S_2CNEt_2)·3H_2O$; 14 g) in 30 mL of methanol was added to europium chloride hexahydrate ($EuCl_3·6H_2O$; 5.6 g) dissolved in 30 mL of methanol with stirring and reacted for 3 h. After the reaction mixture was filtered, a solution of $BrPPh_4$ (6.4 g) in 30 mL of methanol was added to the filtered solution and stirred for 9 h. The resulting precipitate was separated by filtration and washed two times with ethanol. Orange powder. Yield: 30%. FT-IR spectrum (KBr): 2960 (C−H), 1485−1482 (C−N), 1442 (P-phenyl), 1113 (C−S) cm^{-1}. ^{1}H NMR spectrum (CD_3Cl): δ 7.91 (4H, t, J = 6.3 Hz, $[Eu(S_2CNEt_2)_4]$ $(P(C_6H_5)_4(p))$, 7.70 (16H, m, $[Eu(S_2CNEt_2)_4]$ $(P(C_6H_5)_4(o, m))$, 3.17 (8H, q, J = 7 Hz, $[Eu(S_2CNCH_2CH_3)_4]$ (PPh_4)). 1.61 (12H, q, J = 7 Hz, $[Eu(S_2CNCH_2CH_3)_4]$ (PPh_4)). Anal. Calcd for $C_{44}H_{60}EuN_4PS_8$: C, 48.79; H, 5.55; N, 5.06. Found: C, 48.53, H, 5.93, N, 5.15.

Synthesis of Bis(diethyldithiocarbamate)manganese, $[Mn(S_2CNEt_2)_3]$. A solution of sodium dithicarbamate trihydrate ($Na(S_2CNEt_2)·3H_2O$; 2.5 g) in 10 mL of ethanol was added to manganese chloride tetrahydrate ($MnCl_2·4H_2O$; 0.95 g) dissolved in 10 mL of ethanol with stirring and reacted for 1 h. The resulting precipitate was separated by filtration and washed two times with ethanol. Deep-brown powder. Yield: 79%. FT-IR spectrum (KBr): 2974 (C−H), 1485 (C−N), 995 (C−S) cm^{-1}. ^{1}H NMR spectrum (CD_3Cl): δ 4.02 (8H, br, $[Mn(S_2CNCH_2CH_3)_2]$). 1.51 and 1.31 (12H, br, $[Mn(S_2CNCH_2CH_3)_2]$). Anal. Calcd for $C_{10}H_{20}MnN_2S_4$: C, 36.05; H, 6.12; N, 8.41. Found: C, 36.63, H, 6.12, N, 8.44.

Synthesis of Bis(diethyldithiocarbamate)iron, $[Fe(S_2CNEt_2)_3]$. The Fe(II) dithiocarbamate complex was obtained using the same method as for the Mn(II) dithiocarbamate complex. Black powder. Yield: 75%. FT-IR spectrum (KBr): 2976 (C−H), 1491 (C−N), 990 (C−S) cm^{-1}. ^{1}H NMR spectrum (CD_3Cl): δ 4.04 (8H, br,

dx.doi.org/10.1021/ja3106253 | J. Am. Chem. Soc. 2013, 135, 2659−2666

$[Fe(S_2CNCH_2CH_3)_2]$). 1.48 and 1.38 (12H, br, $[Fe(S_2CNCH_2CH_3)_2]$). Anal. Calcd for $C_{10}H_{20}FeN_2S_4$: C, 35.99; H, 6.04; N, 8.39. Found: C, 35.80, H, 5.95, N, 8.39.

Synthesis of Bis(diethyldithiocarbamate)cobalt, [Co-(S_2CNEt_2)$_2$]. The Co(II) dithiocarbamate complex was obtained using the same method as for the Mn(II) dithiocarbamate complex. Green powder. Yield: 75%. FT-IR spectrum (KBr): 2977 (C−H), 1492 (C−N), 1002 (C−S) cm^{-1}. ^1H NMR spectrum (CD_3Cl): δ 3.81 and 3.60 (8H, br, $[Co(S_2CNCH_2CH_3)_2]$). 1.55 and 1.25 (12H, br, $[Fe(S_2CNCH_2CH_3)_2]$). Anal. Calcd for $C_{10}H_{20}CoN_2S_4$: C, 33.79; H, 5.67; N, 7.88. Found: C, 33.63, H, 5.67, N, 7.79.

Synthesis of EuS Nanocrystals with Transition-Metal Ions. Under an N_2 atmosphere, $(PPh_4)[Eu(S_2CNEt_2)_4]$ (0.54 g) and $[Mn(S_2CNEt_2)_3]$ (0.024 g) were dissolved into oleylamine (4.86 g), and the mixture was heated at 140 °C and stirred for 10 min. After the reaction solvent was heated to 300 °C and stirred for 6 h, the obtained purple liquid was centrifuged at 5000 rpm for 10 min. Prepared EuS:Mn nanocrystals were added to 8 mL of toluene and centrifuged at 13000 rpm for 15 min, and a clear purple liquid was obtained by elimination of the deposit. EuS:Fe and EuS:Co nanocrystals were prepared using the same method as for the EuS:Mn nanocrystals.

Preparation of Polymer Thin Films Containing EuS Nanoparticles and Faraday Rotation Measurements. The obtained EuS nanocrystals with transition-metal ions (2 mg) were added to a chloroform solution (8 mL) of poly(methyl methacrylate) (PMMA; 2.0 g) and dispersed well under ultrasonic treatment, giving a colloidal suspension. PMMA thin films were prepared on a glass substrate from the colloidal suspension via a casting method for the Faraday rotation measurements.

The Faraday effect measurements were performed using a measurement system for Faraday and Kerr effects (JASCO, Model K-250). A Xe lamp was used as the light source. The external magnetic field was 15000 Oe.

RESULTS AND DISCUSSION

Preparation of EuS Nanocrystals with Transition-Metal Ions. The EuS nanocrystals composed of Eu(II) ions were prepared by thermal reduction of the single-source precursor $(PPh_4)[Eu(S_2CNEt_2)_4]$ at controlled reaction times and temperatures.[22,23] We also confirmed that transition-metal sulfide nanocrystals, $M^{II}S$, were obtained by the decomposition of the divalent transition-metal precursor, $[M(S_2CNEt_2)_2]$, at 300 °C for 6 h (see the Supporting Information: preparation, Figures S1 and S2). The transition-metal precursors are promising chemical sources for the preparation of EuS nanocrystals with transition-metal ions. We attempted to synthesize these using an oleylamine solution containing $(PPh_4)[Eu(S_2CNEt_2)_4]$ and $[M(S_2CNEt_2)_2]$ at 300 °C for 6 h. XRD spectra of the prepared powders are shown in Figure 2.

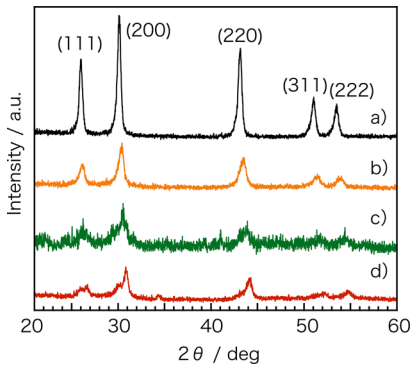

Figure 2. XRD profiles of (a) EuS, (b) EuS:Fe, (c) EuS:Co, and (d) EuS:M nanocrystals.

The 2θ diffraction peaks of the XRD measurements were very similar to those of the corresponding (111), (200), (220), (222), (400), (420), and (422) signals of NaCl type EuS. The slight shifts in the diffraction peaks are due to lattice mismatch of Eu−S by doping transition-metal ions as an impurity. We estimated the lattice constants of the obtained EuS nanocrystals with transition-metal ions using the diffraction peaks of the corresponding diffraction (200) peak in the EuS crystal lattice. The percentage of lattice mismatch is calculated by

$$\text{lattice mismatch} = 100 \times (d^{\text{matrix}} - d^{\text{matrix with dopant}})/d^{\text{matrix}} \quad (1)$$

where d^{matrix} and $d^{\text{matrix with dopant}}$ are lattice constants of the matrix and the matrix with a dopant, respectively.[45] The lattice constants and mismatch percentages of EuS nanocrystals with manganese, cobalt, and iron ions, EuS:Mn, EuS:Fe, and EuS:Co nanocrystals, are summarized in Table 1. The lattice mismatch

Table 1. Lattice Constants, Lattice Mismatch, Crystal Sizes, and Dopant Percentages of EuS, EuS:Mn, EuS:Fe, and EuS:Co Nanocrystals

sample	lattice constant (Å)	lattice mismatch[a] (%)	crystal grain size from XRD[b] (nm)	cryst size from TEM (nm)	dopant ions from ICP-AES (%)
EuS	0.593	0.00	19.9	27.2	0.0
EuS:Mn	0.579	2.62	19.6	26.6	30
EuS:Fe	0.588	0.843	20.3	27.4	4.7
EuS:Co	0.586	1.18	19.4	26.2	17

[a]The lattice mismatch is estimated by eq 1. [b]The crystal grain size is given by calculations using Scherrer's equation.

of EuS:Mn nanocrystals is larger than those of EuS:Co and EuS:Fe. Generally, lattice mismatch of a semiconductor with dopants is related to the amount of dopant ions. The lattice mismatch analysis indicates that the amount of Mn(II) ions in the EuS:Mn crystal grain is greater than those of Fe(II) in EuS:Fe and Co(II) in the EuS:Co crystal grain. The crystal grain size of EuS, EuS:Mn, EuS:Co, and EuS:Fe calculated using the Scherrer equation from the corresponding (200) diffraction peak was found to be 19.9, 19.6, 20.3, and 19.4 nm, respectively (Table 1).

Figure 3 shows TEM images of EuS, EuS:Mn, EuS:Co, and EuS:Fe nanocrystals. Rugged nanocrystals of EuS:Mn, EuS:Co, and EuS:Fe were observed, although the EuS nanocrystals showed a smooth surface with clear facets. The average sizes of the EuS, EuS:Mn, EuS:Co, and EuS:Fe nanocrystals were estimated from the TEM images to be 27.2, 26.2, 27.4, and 26.6 nm, respectively (see Table 1). The average sizes are larger than crystal grain sizes calculated from Scherrer's equation. These size estimations indicate that the EuS nanocrystals with transition-metal ions are covered with an amorphous inorganic layer with a ragged surface.

To determine the amount of transition-metal ions in the EuS nanocrystals, ICP-AES of EuS:Mn, EuS:Co, and EuS:Fe was carried out in nitric acid, for dissolution of the nanocrystals. The percentages of transition-metal ions in the EuS obtained using ICP-AES are summarized in Table 1. The EuS:Mn nanocrystals contain a large amount of elemental Mn (30%), larger than the fraction in the EuS:Co (17%) and EuS:Fe (4.7%) nanocrystals. In the EuS nanocrystals with transition-metal ions, the Eu(II) ion is partially replaced by divalent transition-metal ions, M(II), resulting in the formation of M^{II}−

dx.doi.org/10.1021/ja3106253 | J. Am. Chem. Soc. 2013, 135, 2659−2666

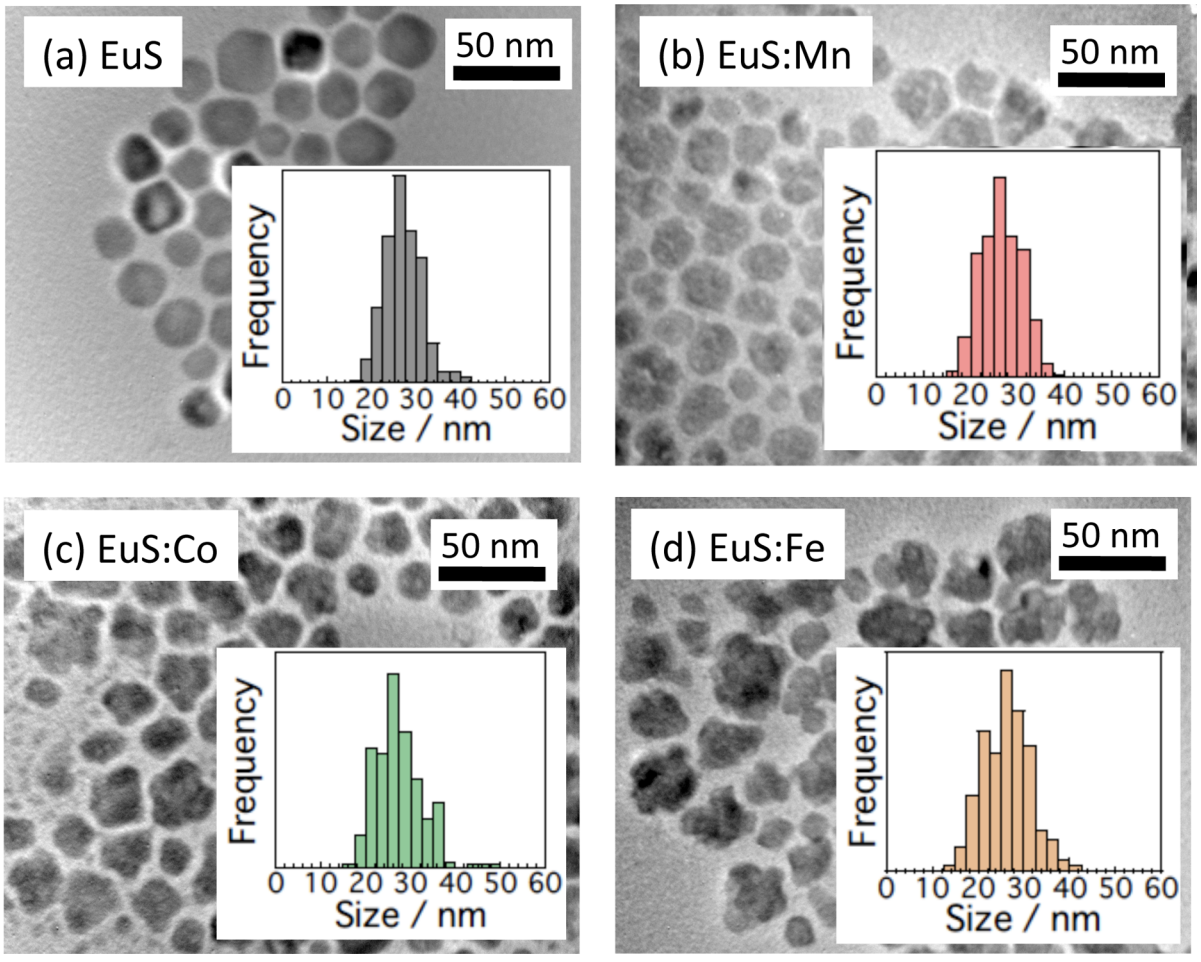

Figure 3. TEM images and size distribution histograms (inset) of (a) EuS, (b) EuS:Mn, (c) EuS:Co, and (d) EuS:Fe nanocrystals.

S bonds. The crystal lattice composed of Mn^{II}–S bonds yields the single manganese sulfide MnS with an NaCl type cubic structure. In contrast, the crystal lattice containing Co^{II}–S bonds yields various types of cobalt sulfides with cubic and hexagonal structures, such as Co_3S_4, $CoS_{1.035}$, $Co_{1-x}S$, Co_4S_3, and β-$CoS_{1.097}$ crystals. The crystal lattice constructed by the Fe^{II}–S bonds also exhibits three types of iron sulfides, FeS, with hexagonal, monoclinic, and tetragonal structures. We consider that the large amount of Mn(II) ions in the EuS:Mn nanocrystals might be due to the stable formation of single and uniform Mn^{II}–S bonds in the cubic EuS lattice, formed homogeneously.

Magnetic Properties. The magnetic properties of EuS, EuS:Mn, EuS:Co, and EuS:Fe nanocrystals were determined from SQUID measurements (Figure 4 and Table 2). The EuS nanocrystals turned into the ferromagnetic phase at 17 K, consistent with the Curie point of the bulk EuS single crystal. The magnetic moment per Eu(II) ion at 5 K was 2.9 μ_B, smaller than the expected value of 7.0 μ_B for the $^8S_{7/2}$ state of Eu(II) at 0 K. In the range 10–100 nm, ferromagnetic nanocrystals are usually composed of a single domain structure. The scale of 20 nm is probably effective in creating a single domain structure in the EuS nanocrystals. However, the complicated morphology of the EuS nanocrystals was considered to affect the magnetic moment, because the disordered arrangement of tiny crystals on the surface of the nanocrystals possibly decreases the exchange interaction between Eu(II) ions.

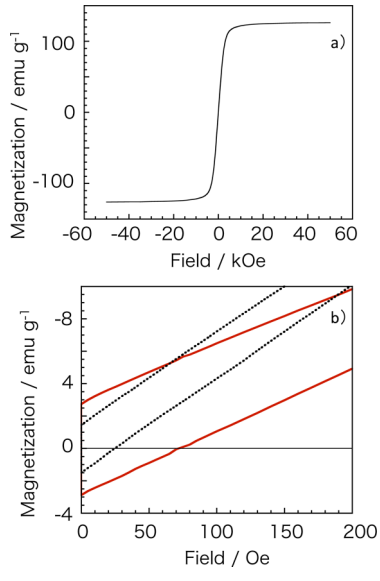

Figure 4. Magnetic field dependences of EuS (a and b, black dotted lines) and EuS:Mn nanocrystals (b, red bold lines).

The Curie points and magnetic moments per Eu(II) ion at 5 K of the EuS:M nanocrystals are smaller than those of the EuS nanocrystals. The smaller Curie points and magnetic moments are due to the complicated morphology on the surface of the nanocrystals. The presence of disordered tiny crystals and

dx.doi.org/10.1021/ja3106253 | J. Am. Chem. Soc. 2013, 135, 2659–2666

Table 2. Magnetic Properties of EuS, EuS:Mn, EuS:Fe, and EuS:Co Nanocrystals

sample	Curie temp (K)	magnetic moment per Eu(II) ion[a] (μ_B)	coercive field[a] (Oe)
EuS	17.5	2.9	25
EuS:Mn	14.0	1.3	70
EuS:Fe	15.0	0.86	40
EuS:Co	15.0	0.80	30

[a]The magnetic moment per Eu(II) ion and coercive field are estimated under 5 K.

oxidized Eu(III) ions on the EuS:M surface might contribute to a decrease in their magnetic moments. The Curie points may also be affected by a lattice mismatch of EuS nanocrystals with transition-metal ions. These results indicate that impurities, such as a transition-metal ion, led to a decrease in the intrinsic magnetic moment of the EuS crystal lattice.

In contrast, we observed that the coercive field of the EuS nanocrystals is enhanced by the addition of transition-metal ions in the EuS crystal lattice. In particular, the coercive field of the EuS:Mn nanocrystals is approximately 3 times larger than that of the EuS nanocrystals. In the case of semiconductor nanocrystals with transition-metal ions, the coercive field is strongly dependent on the ferromagnetic dipole interaction between metal ions. Chaudret et al. have reported that highly ordered assembling of cube-shaped magnetic nanocrystals indicates a strong ferromagnetic dipole interaction between the nanocrystals.[46] We consider that the larger coercive field of the EuS nanocrystals with transition-metal ions might be due to a strong magnetic dipole interaction between Eu(II) and the transition-metal ions. A strong magnetic dipole interaction is directly linked to enhancement of spin polarization in the ground and excited states of the EuS nanocrystals. EuS nanocrystals with large coercive field, EuS:Mn and EuS:Fe, are expected to exhibit large Faraday rotations under a magnetic field.

Magneto-optical Properties. Absorption spectra of EuS:M nanocrystals in toluene are shown in Figure 5a. The characteristic absorption band of EuS is observed at around 550 nm and can be assigned to the 4f–5d ($^4f_7(^8S_{7/2})$–$^4f_6(^7F_J)5d$-(t_{2g},e_g)) transition bands. The energy gap band of the EuS compounds, respectively.[19] These transition bands also indicate the formation of EuS nanocrystals. According to the absorption spectrum of EuS:M nanocrystals, we observed that the wavelengths of the 4f–5d transition bands are slightly blue-shifted, in comparison with the EuS nanocrystals (Figure 5a). The absorption wavelength of the 4f–5d transition bands is summarized in Table 3. The crystal grain sizes of EuS:Mn, EuS:Fe, and EuS:Co nanocrystals using Scherrer's equation are very similar to those of the prepared EuS nanocrystals (Table 1). The characteristic blue shift of the 4f–5d transition bands of EuS:M nanocrystals might be due to the effect of Zeeman splitting in the excited state of EuS with paramagnetic transition-metal ions.

The wavelength dependence of the Faraday rotation angle was measured for PMMA (poly(methyl methacrylate)) thin films containing EuS, EuS:Mn, EuS:Fe, or EuS:Co (Figure 5b and Table 3). The Faraday spectrum at room temperature with 15000 Oe had clear positive and negative peaks, which could have contributed to the 4f–5d transitions of the EuS nanocrystals. The wavelength of the positive peaks for the EuS:M nanocrystals is blue-shifted in comparison to that of the

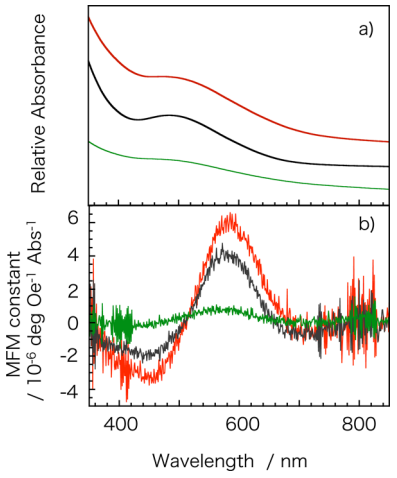

Figure 5. (a) Absorption and (b) Faraday rotation spectra of polymer thin film EuS:Mn (red line), EuS:Co (green line), and EuS:Fe nanocrystals (black line). The concentration of nanocrystals in polymer films was 1 wt %. The thicknesses of thin films using a laser scanning microscope of PMMA containing EuS, EuS:Mn, EuS:Fe, and EuS:Co nanocrystals are found to be 87, 84, 84, 84, and 84 μm, respectively.

Table 3. Faraday Rotation Wavelengths and Verdet Constants of PMMA Thin Films Containing EuS, EuS:Mn, EuS:Fe, and EuS:Co Nanocrystals

sample	absorption wavelength of 4f–5d transition band (nm)	positive peak wavelength of Faraday rotation (nm)	MFM constant at positive peak wavelength[a] ($\times 10^{-6}$ deg Oe)	line width of EPR spectra, ΔH (mT)
EuS	504	599	3.9	96.9
EuS:Mn	501	584	6.1	75.8
EuS:Fe	485	572	4.2	86.3
EuS:Co	480	568	0.9	89.9

[a]MFM constant: absorption-normalized Veldet constant. MFM constant is calculated by eq 3. Thickness of thin films using laser scanning microscope of PMMA containing EuS, EuS:Mn, EuS:Fe, EuS:Co nanocrystals are found to be 87, 84, 84, 84, and 84 μm, respectively.

EuS nanocrystals, which is related to the absorption spectra (Table 3). The Verdet constant, which indicates the strength of the Faraday rotation, is calculated using eq 2:

$$V = \theta/Hl \tag{2}$$

where θ, H, and l are the Faraday rotation angle (degrees), the external magnetic field, and the thickness of the thin film (cm), respectively. The Faraday rotation angle is dependent on the concentration of the Eu(II) ion with magnetic spins. The amount of characteristic Eu(II) ions in the EuS nanocrystals with transition-metal ions is related to the absorption coefficient of the 4f–5d electronic transition. In order to estimate the Faraday rotation efficiency of the nanocrystals, we consider that the Verdet constant should be normalized by the photon-absorption ability of the nanocrystals, which contains information on the absorption coefficient ε, concentration c, and optical pass length l. The magneto-optical figure of merit (MFM) can be rewritten as

$$\mathrm{MFM} = \theta/(H \times A) \tag{3}$$

dx.doi.org/10.1021/ja3106253 | J. Am. Chem. Soc. 2013, 135, 2659–2666

where A is the absorbance of the PMMA film containing EuS and EuS:M(II) nanocrystals. The refractive index of PMMA is 1.48, which is much smaller than that of EuS materials (n = 2.43).[47] Circular birefringence of PMMA as a matrix is also much smaller than Faraday rotation of EuS nanocrystals (see the Supporting Information, Figure S3). The double refraction in the PMMA thin films does not affect the Faraday rotations of EuS nanocrystals in the measurement of circular birefringence. The calculated MFM constants are summarized in Table 3. The MFM constants of EuS:Mn and EuS:Fe are larger than those of the EuS nanocrystals. The enhanced MFM constants of EuS:Mn and EuS:Fe nanocrystals in the PMMA thin films may be caused by the their strong ferromagnetic interactions related to their large coercive field. In particular, the MFM constant of the EuS:Mn nanocrystals with a large coercive field is the largest in the EuS nanocrystals with transition-metal ions. In contrast, we also observed a decrease in the Faraday rotation angle of the EuS:Co nanocrystals. Amplification of the coercive field of the EuS:Co nanocrystals is smaller than that of the EuS:Fe nanocrystals, although the percentage of Co(II) ions from ICP-AES is much larger than that of Fe(II) ions in the EuS nanocrystals. Here, we propose that the Faraday rotation of the EuS:M nanocrystals can be directly linked to the coercive field, which leads to enhancement of ferromagnetic exchange interaction and spin polarization in the ground and excited states of the EuS nanocrystals.

According to the spin polarization on the magneto-optical effect, Wachter and co-workers previously suggested their skew scattering model.[48] The theoretical model is based on the asymmetric spin−orbit interaction, which is estimated using conductivity considering an electric field and assuming a relaxation lifetime approximation. The relaxation lifetime for spin−orbit asymmetric scattering is one of the key factors in the parameters of magneto-optical effect, off-diagonal elements in the optical conductivity tensor σ^2_{xy}. We consider that the asymmetric spin−orbit interaction in the past theoretical model might be linked to our experimental data and related to the spin polarization in EuS:M nanocrystals. On the other hand, Erskine and Stern have focused on the minority spin electron in magnetic materials.[49] Minority spin transitions of the magnetic materials produce the first negative peak and second positive peak in magneto-optical rotation spectra. At the present time, measurement and calculation of the spin polarization or minority spin electron in optical transition is not clear in our present EuS:M nanocrystals. However, asymmetric spin−orbit interaction and spin polarization of EuS:M in the optical transition might promote enhancement of the optical conductivity tensor σ^2_{xy} and Faraday effects.

Estimation of Ferromagnetic Exchange Interaction using EPR Spectra. The ferromagnetic exchange interaction is a key factor for understanding the optical Faraday rotation of EuS:M nanocrystals. The ferromagnetic exchange interaction, H_e, is given by

$$\Delta H_{1/2} = H_d^2/H_e \quad (4)$$

where H_d and $\Delta H_{1/2}$ are terms of magnetic dipole interaction and fwhm (full width at half-maximum) of the EPR signal, respectively. H_e can be estimated from the $\Delta H_{1/2}$ value usingthe line width ΔH of observed EPR spectra (differential form).[50]

Thus, in order to estimate the ferromagnetic exchange interaction of the EuS nanocrystals with transition-metal ions, we carried out EPR measurements. The EPR spectra are shown in Figure 6. The line widths ΔH of the EPR spectra are summarized in Table 3. The EPR spectra provide the typical

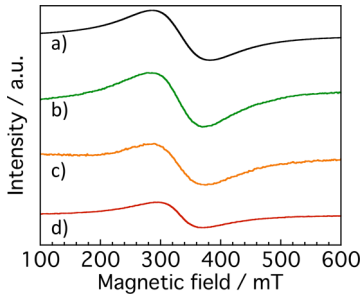

Figure 6. Normal and differential EPR spectra of EuS (a, black line), EuS:Co (b, green line), EuS:Fe (c, orange), and EuS:Mn nanocrystals (d, red line).

spin configuration of Eu(II) ions in the EuS crystal. ΔH calculated using the EPR spectrum of the EuS:Mn nanocrystals is found to be 75.8 mT, which is the smallest value obtained in our experiments. The ferromagnetic exchange interaction in the EuS:Mn nanocrystals is much stronger than that in the EuS nanocrystals. For the first time, we successfully observed the intrinsic driving force, the ferromagnetic exchange interaction, for understanding the Faraday effect. On the other hand, the EPR measurement of EuS:Co gives a large ΔH value of 89.9 mT.

Generally, the magnetic dipole interaction H_d is directly linked to the distance between magnetic ions. The distance between Eu(II) ions in EuS:Mn using XRD analysis is longer than in EuS:Co. However, the line width of the EPR signal of EuS:Mn with a smaller magnetic dipole interaction, ΔH of EuS:Mn, is narrow. The small magnetic dipole interaction by doping of Mn(II) ions is supported by a previous study.[51] We think that the magnetic dipole interaction H_d is not subject to the influence of ferromagnetic interaction, directly. A magnetic material with a narrower ΔH value provides a larger ferromagnetic exchange interaction.[45] The Mn(II) ion promotes effective enhancement of the ferromagnetic exchange interaction in the EuS nanocrystals. The ferromagnetic exchange interaction in the EuS nanocrystals is dependent on the species of transition-metal ion used as the dopant. The small Faraday rotation angle of the EuS:Co nanocrystals might be not only due to small enhancement of the ferromagnetic exchange interaction but also due to the decrease of the intrinsic magnetic moment of the EuS crystal lattice as an impurity. From these results, we conclude that the magneto-optical effect, the Faraday rotation, is affected by the ferromagnetic exchange interaction related to the coercive field of magnetic materials.

SUMMARY AND CONCLUSIONS

EuS nanocrystals with paramagnetic transition-metal ions, EuS:M, were successfully prepared by the reaction of a Eu(III) dithiocarbamate complex with Mn(II), Fe(II), and Co(II) complexes. Their Faraday rotation angles depended on the species of transition-metal ion used as a dopant. In particular, a PMMA thin film containing EuS:Mn nanocrystals showed effective Faraday rotation under a magnetic field. In this study, we also suggested that the large Faraday rotation efficiency is based on the ferromagnetic exchange interaction related to the characteristic coercive field of EuS:Mn nanocrystals. The

dx.doi.org/10.1021/ja3106253 | J. Am. Chem. Soc. 2013, 135, 2659−2666

intrinsic effect of the ferromagnetic exchange interaction on magneto-optical properties is a new aspect for the development of magnetic semiconductors, although the magnetic moment and Curie point of a magnetic semiconductor have been previously examined.

This study is significant in that it is directly related to photophysical chemistry and future photofunctional materials science research. EuS:M with enhanced magnetic and magneto-optical properties is expected to be useful in applications such as novel optical isolators and spintronic devices.

■ ASSOCIATED CONTENT

Supporting Information

XRD profile of MnS (Figure S1), TEM image and average size of MnS nanocrystals (Figure S2), Faraday rotation spectra of PMMA without EuS nanocrystals (Figure S3), and text giving details of the syntheses of MnS, CoS, and FeS nanocrystals. This material is available free of charge via the Internet at http://pubs.acs.org.

■ AUTHOR INFORMATION

Corresponding Author

hasegaway@eng.hokudai.ac.jp.

Notes

The authors declare no competing financial interest.

■ ACKNOWLEDGMENTS

We are grateful to Mr. Akira Kawashima, Graduate School of Engineering, Hokkaido University, for the Faraday rotation measurements. This work was partly supported by Grants-in-Aid for Scientific Research on Innovative Areas of "Emergent chemistry of nano-scale molecular systems" and "New Polymeric Materials Based on Element-Blocks (No. 2401)" (24102012) of the Ministry of Education, Culture, Sports, Science and Technology (MEXT) of Japan.

■ REFERENCES

(1) Furdyna, J. K. *J. Appl. Phys.* **1988**, *64*, R29−R64.
(2) Gaj, J. A.; Ginter, J.; Galazka, R. R. *Phys. Status Solidi B: Basic Res.* **1978**, *89*, 655−662.
(3) Ohno, H.; Shen, A.; Matsukura, F.; Oiwa, A.; Endo, A.; Katsumoto, S.; Iye, Y. *Appl. Phys. Lett.* **1996**, *69*, 363−365.
(4) Ohno, Y.; Young, D. K.; Beschten, B.; Matsukura, F.; Ohno, H.; Awschalom, D. D. *Nature* **1999**, *402*, 790−792.
(5) Jungwirth, T.; Atkinson, W. A.; Lee, B. H.; MacDonald, A. H. *Phys. Rev. B* **1999**, *59*, 9818−9821.
(6) Wang, Y.; Herron, N.; Moller, K.; Bein, T. *Solid State Commun.* **1991**, *77*, 33−38.
(7) Norris, D. J.; Yao, N.; Charnock, F. T.; Kennedy, T. A. *Nano Lett.* **2001**, *1*, 3−7.
(8) Jun, Y. W.; Jung, Y. Y.; Cheon, J. *J. Am. Chem. Soc.* **2002**, *124*, 615−619.
(9) Schwartz, D. A.; Norberg, N. S.; Nguyen, Q. P.; Parker, J. M.; Gamelin, D. R. *J. Am. Chem. Soc.* **2003**, *125*, 13205−13218.
(10) Stowell, C. A.; Wiacek, R. J.; Saunders, A. E.; Korgel, B. A. *Nano Lett.* **2003**, *3*, 1441.
(11) Norberg, N. S.; Kittilstved, K. R.; Amonette, J. E.; Kukkadapu, R. K.; Schwartz, D. A.; Gamelin, D. R. *J. Am. Chem. Soc.* **2004**, *126*, 9387−9398.
(12) Erwin, S. C.; Zu, L.; Haftel, M. I.; Efros, A. L.; Kennedy, T. A.; Norris, D. J. *Nature* **2005**, *436*, 91−94.
(13) Beaulac, R.; Archer, P. I.; Liu, X.; Lee, S.; Salley, G. M.; Dobrowolska, M.; Furdyna, J. K.; Gamelin, D. R. *Nano Lett.* **2008**, *8*, 1197−1201.
(14) Wachter, P. *Handbook on the Physics and Chemistry of Rare Earths*, 2nd ed.; North-Holland: Amsterdam, 1979; CRC Critical Reviews in Solid State Science, pp 189−241.
(15) Suits, J. C.; Argyle, B. E.; Freiser, M. J. *J. Appl. Phys.* **1966**, *37*, 1391−1397.
(16) Hasegawa, Y.; Thongchant, S.; Wada, Y.; Tanaka, H.; Kawai, T.; Sakata, T.; Mori, H.; Yanagida, S. *Angew. Chem., Int. Ed.* **2002**, *41*, 2073−2075.
(17) Thongchant, S.; Hasegawa, Y.; Wada, Y.; Yanagida, S. *J. Phys. Chem. B* **2003**, *107*, 2193−2196.
(18) Hasegawa, Y.; Afzaal, M. A.; O'Brien, P.; Wada, Y.; Yanagida, S. *Chem. Commun.* **2005**, 242−243.
(19) Kataoka, T.; Tsukahara, Y.; Hasegawa, Y.; Wada, Y. *Chem. Commun.* **2005**, 6038−6040.
(20) Hasegawa, Y.; Okada, Y.; Kataoka, T.; Sakata, T.; Mori, H.; Wada, Y. *J. Phys. Chem. B* **2006**, *110*, 9008−9011.
(21) Hasegawa, Y.; Adachi, T.; Tanaka, A.; Afzaal, M.; O'Brien, P.; Doi, T.; Hinatsu, Y.; Fujita, K.; Tanaka, K.; Kawai, T. *J. Am. Chem. Soc.* **2008**, *130*, 5710−5715.
(22) Tanaka, A.; Kamikubo, H.; Doi, Y.; Hinatsu, Y.; Kataoka, M.; Kawai, T.; Hasegawa, Y. *Chem. Mater.* **2010**, *22*, 1776−1781.
(23) Tanaka, A.; Kamikubo, H.; Kataoka, M.; Hasegawa, Y.; Kawai, T. *Langmuir* **2011**, *27*, 104−108.
(24) Regulacio, M. D.; Tomson, N.; Stoll, S. L. *Chem. Mater.* **2005**, *17*, 3114−3121. (b) Zhao, F.; Sun, H.; Gao, S.; Su, G. *J. Mater. Chem.* **2005**, *15*, 4209−4214.
(25) Mirkovic, T.; Hines, M. A.; Sreekumari, Nair P.; Scholes, G. D. *Chem. Mater.* **2005**, *17*, 3451−3456.
(26) Regulacio, M. D.; Bussmann, K.; Lewis, B.; Stoll, S. L. *J. Am. Chem. Soc.* **2006**, *128*, 11173−11179.
(27) Zhao, F.; Sun, H.-L.; Su, G.; Gao, S. *Small* **2006**, *2*, 244−248.
(28) Huxter, V. M.; Mikovic, T.; Nair, P. S.; Scholes, G. D. *Adv. Mater.* **2008**, *20*, 2439−2443.
(29) Regulacio, M. D.; Kar, S.; Zuniga, E.; Wang, G.; Dollahon, N. R.; Yee, G. T.; Stoll, S. L. *Chem. Mater.* **2008**, *20*, 3368−3376.
(30) Pereira, A. S.; Rauwel, R.; Reis, M. S.; Silva, N. J. O; Barros-Timmons, A.; Trindade, T. *J. Mater. Chem.* **2008**, *18*, 4572−4578.
(31) Selinsky, R. S.; Keavney, D. J.; Bierman, M. J.; Jin, S. *Appl. Phys. Lett.* **2009**, *95*, 202501.
(32) Kar, S.; Boncher, W. L.; Olszewski, D.; Dollahon, N.; Asdh, R.; Stoll, S. L. *J. Am. Chem. Soc.* **2010**, *132*, 1360−13962.
(33) Selinsky, R. S.; Han, J. H.; Perez, E. A. M.; Guzei, I. A.; Jin, S. *J. Am. Chem. Soc.* **2010**, *132*, 15997−16005.
(34) He, W.; Dickerson, J. H. *Appl. Phys. Lett.* **2011**, *98*, 081914−1−3.
(35) Kar, S.; Dollahon, N. R.; Stoll, S. L. *J. Solid State Chem.* **2011**, 1324−1327. (l) He, W. D.; Somarajan, S.; Koktysh, D. S.; Dickerson, J. H. *Nanoscale* **2011**, *3*, 184−187.
(36) Moruzzi, V. L.; Teaney, D. T.; van der Hoeven, B. J. C., Jr. *Solid State Commun.* **1968**, *6*, 461−464.
(37) Gambino, R. J.; Fumagalli, P.; Ruf, R. R.; McGuire, T. R.; Bojarczuk, N. *IEEE Trans. Magn.* **1992**, *28*, 2973−2975.
(38) Mauger, A.; Godart, C. *Phys. Rep.* **1986**, *141*, 51.
(39) Pourbaix, M. *Atlas of Electrochemical Equilibria*, 2nd English ed.; National Association of Corrosion Engneers and CEBELCOR: Houston, TX, and Brussels, Belgium, 1974; pp 189−190
(40) Kim, M.-A.; Lee, J.-L.; Jung, J.; Park, J.-K. *Chem. Commun.* **2012**, *48*, 904−906.
(41) Blasse, G.; Grabmaier, B. C. *Luminescent Materials*; Springer-Verlag: New York, 1994.
(42) Eliseeva, S. V.; Bünzli, J.-C. G. *Chem. Soc. Rev.* **2010**, *39*, 189−227.
(43) Hasegawa, Y.; Wada, Y.; Yanagida, S. *J. Photochem. Photobiol. C: Photochem. Rev.* **2004**, *5*, 183−189.
(44) Matsukura, F.; Ohno, H.; Shen, A.; Sugawara, Y. *Phys. Rev.* **1998**, *B57*, R2037.
(45) Nag, A.; Chakraborty, S.; Sarma, D. D. *J. Am. Chem. Soc.* **2008**, *130*, 10605−10611.

(46) Snoeck, E.; Gatel, C.; Lacroix, L. M.; Blon, T.; Lachaize, S.; Carrey, J.; Respaud, M.; Chaudret, B. *Nano Lett.* **2008**, *8*, 4293−4298.
(47) Bachmann, R.; Wachter, P. *J. Appl. Phys.* **1969**, *40*, 1326−1327.
(48) Reim, W.; Hüsser, O. E.; Schoenes, J.; Kaldis, E.; Wachter, P.; Seiler, K. *J. Appl. Phys.* **1984**, *55*, 2155−2157.
(49) Erskine, J. K.; Stern, E. A. *Phys. Rev. Lett.* **1973**, *30*, 1329−1332.
(50) Sagar, R. V.; Buddhudu, S. *Spectrochim. Acta, Part A* **2010**, *75*, 1218−1222.
(51) Chamberlain, S. L.; Corruccini, L. R. *J. Low Temp. Phys.* **2007**, *149*, 7087.